

TiO₂ porous ceramic/Ag–AgCl composite for enhanced photocatalytic degradation of dyes under visible light irradiation

Zhouzhou Feng¹ · Xiang Lv¹ · Tianhe Wang¹ 

Published online: 15 May 2017

© The Author(s) 2017. This article is an open access publication

Abstract TiO₂ porous ceramic/Ag–AgCl composite was prepared by incorporating AgCl nanoparticles within the bulk of TiO₂ porous ceramic followed by reducing Ag⁺ in the AgCl particles to Ag⁰ species under visible light irradiation. The porous TiO₂ ceramic was physically robust and chemically durable, and the porous structure facilitated the implantation of AgCl NPs. Compared with the bare TiO₂ ceramic, TiO₂ porous ceramic/Ag–AgCl composite exhibited higher photocatalytic performance for the degradation of MO and RhB under visible light irradiation. The reaction rate constants *k* of MO and RhB degradation over TiO₂ porous ceramic/Ag–AgCl composite was respectively 6.25 times and 3.62 times higher than those recorded over the bare TiO₂ porous ceramic. The photocatalytic activity showed virtually no decline after four times cyclic experiments under visible light irradiation. Scanning electron microscopy, energy dispersive X-ray analysis, X-ray diffraction, UV–Vis diffuse reflectance spectroscopy, photoluminescence spectra and X-ray photoelectron spectroscopy were used to characterize the TiO₂ porous ceramic/Ag–AgCl composite.

Keywords TiO₂ porous ceramic/Ag–AgCl composite · Porous TiO₂ · Photocatalyst · Visible light

1 Introduction

On the basis of highly efficient photocatalysts and solar energy, environmental purification and energy conversion are attracting great attention [1]. Ever since Fujishima and Honda reported TiO₂ as UV photocatalyst that can split water [2], several new semiconductor photocatalysis has been discovered attracting enormous interests. As an ideal photocatalyst, TiO₂ has been the most investigated photocatalyst because of its exceptional properties including non-toxicity, long-term photochemical stability and low cost [3–6]. However it has large bandgap (3.0 eV for rutile and 3.2 eV for anatase) and this leads to the fact that only ultraviolet in the solar spectrum contributes to photocatalytic effect. Various methods have been proposed and investigated in attempt to extend photocatalysis to the visible range, including doping of metallic [7] or non-metallic elements [8] into TiO₂, coupling with materials sensitive to visible light [9], morphology engineering [10] and adding co-catalysts [11].

Plasmonic photocatalysts, mostly consisted of metal nanoparticles (NPs), exhibit strong photocatalytic activities under visible light due to the surface plasmon resonance effect of the metal NPs. Noble-metal nanoparticles exhibited excellent visible-light absorption because of size- and shape-dependent plasmon resonance, which has a wide range of applications such as colorimetric sensors [12], photovoltaic devices [13] and photocatalysts [14, 15]. According to these reports, the deposition of the metallic species on TiO₂ catalysts improved its photo-efficiency through the Schottky barrier CB electron trapping and consequent longer electron–hole pair lifetimes [16, 17]. Typical plasmonic photocatalysts include Ag/AgX [18, 19] and (Au, Ag)/TiO₂ composites. Ag/AgCl-based photocatalysts have received particular attention, for their outstanding visible-light-responsive photocatalytic performances,

✉ Tianhe Wang
thwang56@126.com

¹ Chemicobiology and Functional Materials Institute, Nanjing University of Science and Technology, Nanjing 210094, People's Republic of China

although silver halide is used as the primary source material in photosensitive plates and is unstable under sunlight [20–22]. Since Huang et al. introduced a new plasmonic photocatalyst Ag@AgCl which is highly efficient and stable under visible light [23], plasmonic photocatalysts has been developed rapidly. Hu et al. synthesized Ag/AgBr@TiO₂ by deposition–precipitation for the destruction of azodyes and bacteria under visible light [24]. Silver halides which are combined with Ag NPs, and particularly TiO₂, have good stability, allowing their application as photocatalysts. Yu et al. prepared Ag/AgCl/TiO₂ nanotube arrays (NTs) by deposition–precipitation for the degradation of MO [25]. Cho et al. reported a one-step sonochemical method to produce Ag/AgCl@TiO₂ nanoparticles by the decomposition of RhB [26]. However, little work has been reported on fabrication of TiO₂ porous ceramic and Ag/AgCl NPs-based composite structures and their photocatalytic activity. In practical applications, bulk photocatalyst is much more needed because it is easily handled in industrial scale applications and circling.

In this paper, we report a TiO₂ porous ceramic/Ag–AgCl composite for photocatalysis. AgCl was dispersed on performed TiO₂ bulk by impregnating TiO₂ matrix in the aqueous solution of Ag(NH₃)₂NO₃ and NaCl, and then reduced partial Ag⁺ in the AgCl particles to Ag⁰ species under visible light irradiation. The visible light driven photocatalytic activity of TiO₂ porous ceramic/Ag–AgCl was investigated for the photocatalytic degradation of MO and RhB. Such composites showed high photocatalytic activity for the degradation of these dyes. The microstructure of the ceramic composite was characterized in detail and the achieved photocatalytic activity was discussed.

2 Experimental section

2.1 Chemicals

Silver nitrate (AgNO₃, ≥99.8%, Sinopharm), sodium chloride (NaCl, ≥99.5%, KeLong Chemical), ammonia solution (NH₃·H₂O, 25–28%, KeLong Chemical), methyl orange (MO, >98%, Alfa Aesar), rhodamine B (RhB, ≥95%, Aladdin) were used as received without additional purification. P25 TiO₂ was from Degussa and colloidal silica (30 wt%) was obtained from Zhejiang Jiahe Chemical Ltd. De-ionized water was used as the solvent in all experiments.

2.2 Preparation of TiO₂ porous ceramic

5 g P25 TiO₂ and 1 g (30 wt%) silica gel were mixed to obtain the dispersed TiO₂ slurry. Then the slurry was placed between two metal plates to be pressed into TiO₂

porous bulk (diameter 25 mm, thickness 2 mm) and sintered at 550 °C for 1 h.

2.3 Preparation of TiO₂ porous ceramic/Ag–AgCl composite

A 200 μL ammonia solution (1 M) was added dropwise to the 10 mL AgNO₃ solution (0.01 M). TiO₂ porous bulk was immersed in the above solution under vacuum for 10 min. Then the bulk was washed with de-ionized water to remove the residual solution. Next, the sample was soaked in 10 mL NaCl solution (0.01 M) for 10 min under vacuum. Subsequently, TiO₂ porous bulk was washed with de-ionized water. Such immersion cycle was repeated three times, and TiO₂ porous ceramic/AgCl was formed. TiO₂ porous ceramic/AgCl was irradiated for a period of time under visible light (a 300 W Xe arc lamp as the visible light source with a 420 nm cutoff filter). The as-prepared composites were denoted as TiO₂ porous ceramic/Ag–AgCl-*n*, where “*n*” represented 10, 20 and 30 min of photo-reduction, respectively.

2.4 Characterization

X-ray diffraction (XRD) measurements were performed on a Bruker D8 advanced diffractometer equipped with Cu Kα radiation source (λ = 1.54056 Å). The samples were examined by obtaining UV–Vis diffuse reflectance spectra (Shimadzu UV 2600). Scanning electron microscopy (SEM, HITACHI S-4800, Japan) was used to observe the surface state and structure of the nanostructured sample. Energy dispersive X-ray spectroscopy (EDX) was used for elemental analysis and distribution of the TiO₂ porous ceramic/Ag–AgCl composite. X-ray photoelectron spectroscopy (XPS) was performed on an RBD upgraded PHI-5000C ESCA system (Perkin-Elmer) with Mg Kα (1253.6 eV) source. All the binding energies were referenced to the contaminant C1s peak at 284.6 eV of the surface of adventitious carbon. The photoluminescence (PL) spectra of 2-hydroxyterephthalic acid at 425 nm were measured using a FL3-TCSPC fluorescence spectrophotometer (Horiba Jobin Yvon, France) by an excitation wavelength of 315 nm.

2.5 Photocatalytic experiment

The photocatalytic activities were evaluated by degradation of MO (10 mg/L) and RhB (10 mg/L) in aqueous solution under visible light (a 300 W Xe arc lamp as the visible light source with a 420 nm cutoff filter) irradiation. Photocatalytic experiments were performed in a glass reactor (diameter = 7 cm, height = 2 cm) and the reactor was placed on the magnetic churn dasher. TiO₂ porous ceramic/

Ag–AgCl (diameter 25 mm, thickness 2 mm) was placed in 25 mL MO or RhB solutions. The system was irradiated under visible light for a fixed period and was equipped with a water-cooling quartz jacket to maintain the solution at room temperature. The distance between the lamp and the reactor was 15 cm. Prior to irradiation, the reaction system was kept for 30 min in the dark to achieve adsorption/desorption equilibrium. During the irradiation, 2 ml of the transparent solution was withdrawn periodically from the reactor and then analyzed by a UV-Vis spectrometer at their characteristic adsorption wavelengths (peak of MO at 464 nm, peak of RhB at 526.5 nm). After the analysis, 2 mL solution was carefully collected and returned to the original reactor. The analysis of $\cdot\text{OH}$ generated on the samples/water interface was performed by PL technique using terephthalic acid. Experimental procedures were identical to that of photocatalytic process. 5×10^{-4} M terephthalic acid aqueous solution in a diluted NaOH aqueous solution with a concentration of 2×10^{-3} M was used to replace the MO or RhB aqueous solution.

3 Results and discussion

3.1 Characterization of photocatalyst

The strategy for the fabrication of TiO_2 porous ceramics/Ag–AgCl is shown in Scheme 1, by a two-step procedure. XRD was used to determine the crystal structure of the photocatalyst. Figure 1 shows the XRD pattern of TiO_2 porous ceramic and TiO_2 porous ceramic/Ag–AgCl composite. TiO_2 displays typical diffraction peaks of TiO_2 anatase phase (JCPDS file no.: 21-1272) [27, 28]. The diffraction peaks at 2θ values of 25.4° , 37.9° , 48.1° , 53.8° , 55.1° and 62.7° could be assigned to the (101), (004), (200), (105), (201) and (204) crystalline phase of anatase TiO_2 . Compared to TiO_2 , the XRD pattern of TiO_2 porous ceramic/Ag–AgCl indicates that additional peaks can be attributed to the cubic phase of AgCl (JCPDS file no.: 31-1238) [19, 23] and metallic Ag (JCPDS file no.: 65-2871) [19]. The

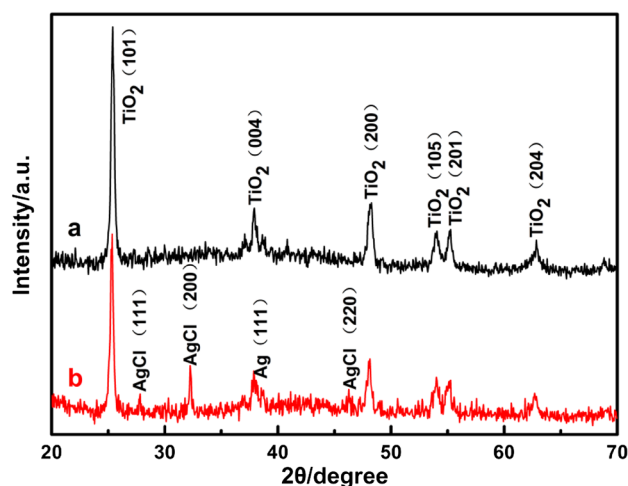
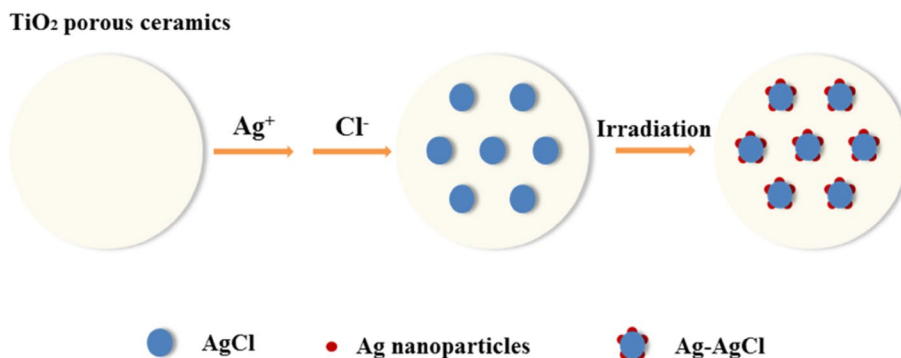


Fig. 1 XRD pattern of *a* TiO_2 porous ceramic and *b* TiO_2 porous ceramic/Ag–AgCl-30

diffraction peaks (2θ) at 27.8° (111), 32.2° (200) and 46.2° (220) are attributed to AgCl. Additionally, the diffraction peaks at 38.2° (111) could be assigned to metallic Ag. Figure 2 shows the UV–Visible diffuse reflectance spectra of TiO_2 porous ceramic and TiO_2 porous ceramic/Ag–AgCl-30. As it can be seen, TiO_2 porous ceramic exhibits low absorptions. While the absorption bands intensified in the 400–750 nm, owing to the surface plasmon resonance of Ag NPs, which were produced by the photo-reduction of AgCl. This further confirms that Ag–AgCl NPs had been deposited successfully on the surface of TiO_2 porous ceramic.

The color of the bulk changed from white to purplish red after visible light irradiation, indicating the formation of Ag NPs, as shown in Fig. 3. The morphology and composition of TiO_2 porous ceramic/Ag–AgCl sample were characterized by SEM and EDX. As shown in Fig. 4a, TiO_2 bulk exhibit a narrow range of particle size distribution with the average particle size around 50 nm. The agglomeration of TiO_2 leads to porous structure that is capable of adsorbing more functional molecules. After AgCl deposition on

Scheme 1 Schematic representation of TiO_2 porous ceramics/Ag–AgCl



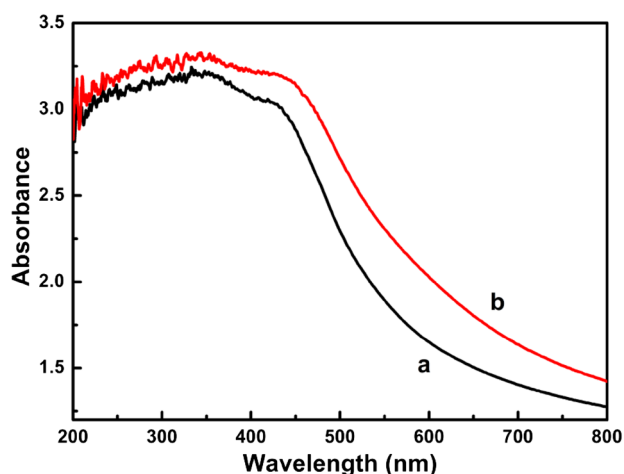


Fig. 2 UV-Visible diffuse reflectance spectra of *a* TiO₂ porous ceramic and *b* TiO₂ porous ceramic/Ag–AgCl-30

TiO₂, the surfaces of TiO₂ became rough as revealed in Fig. 4b–d. Ag–AgCl nanoparticles were cube-like and particle size distribution was regular. It was clearly observed that the average size of Ag–AgCl nanoparticles almost had no change with photo-irradiation time increased. As indicated in Fig. 4, cube-like Ag–AgCl nanoparticles size is about 300 nm. Figure 5 displays the EDX analysis of TiO₂ porous ceramic/Ag–AgCl and shows the element mapping images of O, Si, Cl, Ti and Ag in the composite. These results further confirmed the coexistence of TiO₂ and AgCl without contamination by other chemical species.

The chemical composition and oxidation state of TiO₂ porous ceramic/Ag–AgCl composite was further characterized by XPS spectra (Fig. 6). The survey spectrum in Fig. 6a indicates that four major sets of peaks for Ti 2p, O 1s, Ag 3d and Cl 2p states existed in the sample. The appearance of Si is attributed to silicon from colloidal silica. The Ti 2p spectrum has two obvious peaks at 457.9

and 463.6 eV, belonging to Ti 2p_{3/2} and Ti 2p_{1/2} of Ti⁴⁺ in TiO₂ (Fig. 6b) [29]. In Fig. 6c, the Ag 3d spectrum consists of two sets of peaks: one set is composed of two peaks at about 366.2 and 372.3 eV, which correspond to the Ag 3d_{5/2} and Ag 3d_{3/2} of AgCl, respectively; the other set comprises two weak peaks at about 367.0 and 373.0 eV, which could be attributed to the metallic Ag⁰ [30, 31]. The existence of Ag metal is consistent with the XRD result. Figure 4d shows that two peaks at about 196.5 and 198.1 eV are ascribed to Cl 2p₃ and Cl 2p₁ of AgCl, respectively [32]. The XPS spectra further confirm that TiO₂ porous ceramic/Ag–AgCl composites consist of TiO₂, AgCl and metallic Ag. On the basis of XRD, UV/vis, SEM, EDX and XPS, the Ag–AgCl NPs are dispersedly deposited in the TiO₂ porous bulk.

3.2 Photocatalytic activity

The photocatalytic activity of TiO₂ porous ceramic/Ag–AgCl-*n* (where *n* represents different reduction time for Ag⁺ to Ag⁰) catalysts was evaluated by the degradation of MO (10 mg/L) and RhB (10 mg/L) aqueous solution under visible light irradiation at room temperature. Figure 7 shows the UV-Vis adsorption spectra for the degradation of MO and RhB in the presence of TiO₂ porous ceramic/Ag–AgCl-30. The UV-Vis adsorptions of MO and RhB at their characteristic adsorption wavelengths decrease rapidly with the increase of irradiation time in Fig. 7a, b. Fig. 8a, c shows the degradations (*C/C*₀) of MO and RhB as function of irradiation time with TiO₂ porous ceramic and TiO₂ porous ceramic/Ag–AgCl composites prepared with different reduction time under visible light irradiation, where *C* are the concentrations of MO and RhB varied with irradiation time and *C*₀ are the initial concentrations of dyes. To reach the adsorption equilibrium, the sample is mixed with MO or RhB aqueous solution in the dark for 30 min prior to the photodegradation process. During the period,

Fig. 3 Digital photographs of the **a** TiO₂ porous ceramic and **b** TiO₂ porous ceramic/Ag–AgCl

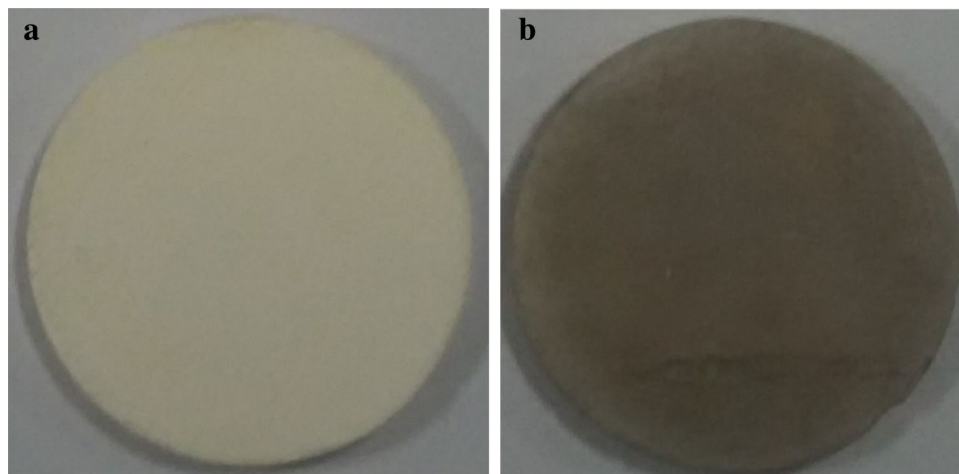


Fig. 4 SEM images of **a** TiO₂ porous ceramic and TiO₂ porous ceramic/Ag–AgCl with different photo-reduction time: **b** 10 min, **c** 20 min and **d** 30 min

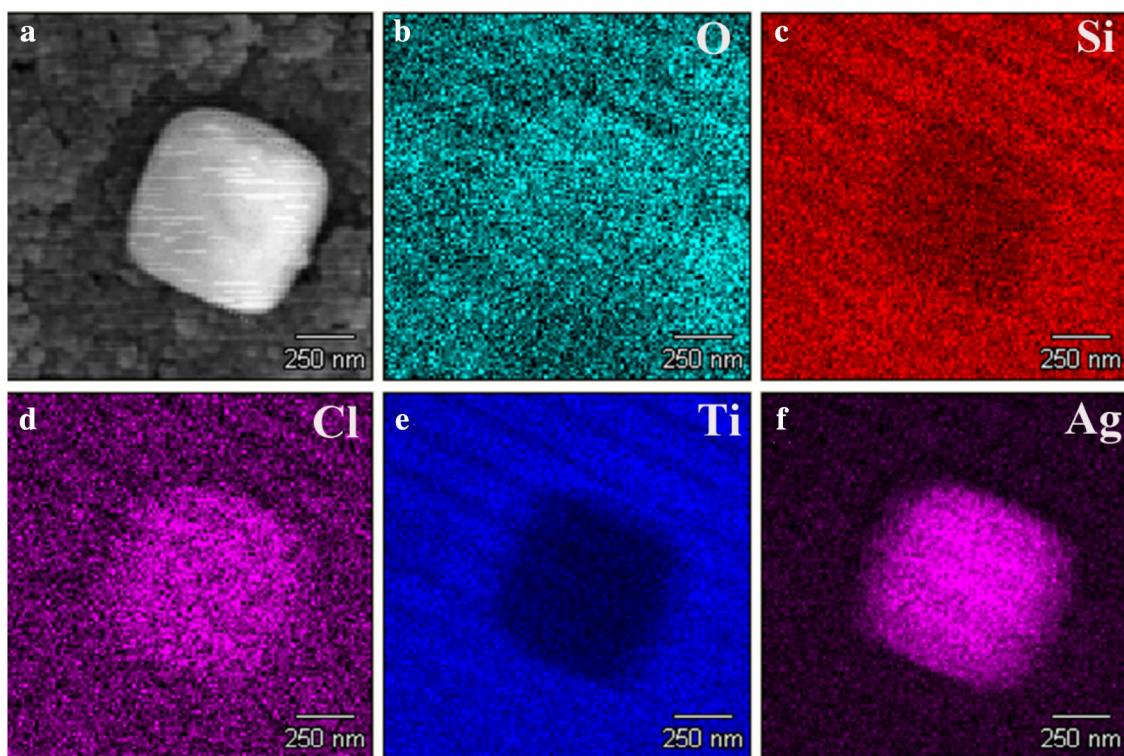
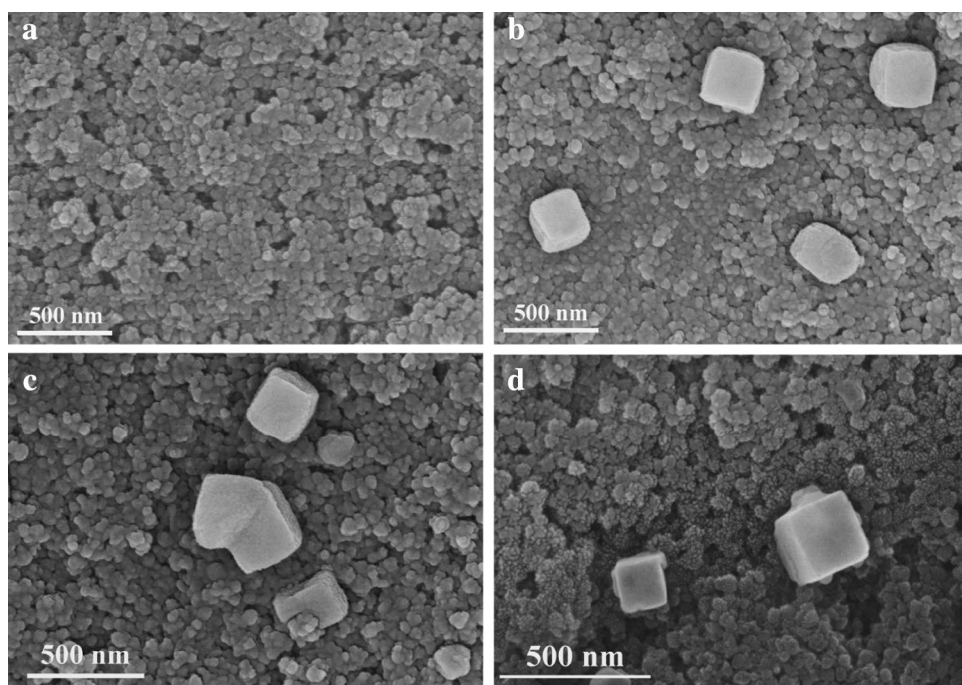


Fig. 5 SEM images of **a** TiO₂ porous ceramic/Ag–AgCl and **b–f** EDS element mapping images of O, Si, Cl, Ti and Ag

only slight reduction in MO and RhB concentrations was observed. Significant degradation of dyes was observed in the present of TiO₂ porous ceramic/Ag–AgCl under visible light irradiation. The photocatalytic activity of TiO₂ porous ceramic/Ag–AgCl catalysts was much higher than

those of TiO₂ bulk. TiO₂ porous ceramic/Ag–AgCl samples with different reduction time exhibited similar photocatalytic activity. For TiO₂ porous ceramic/Ag–AgCl composite, complete degradations of MO and RhB were almost achieved after the 50 and 30 min of irradiation, respectively.

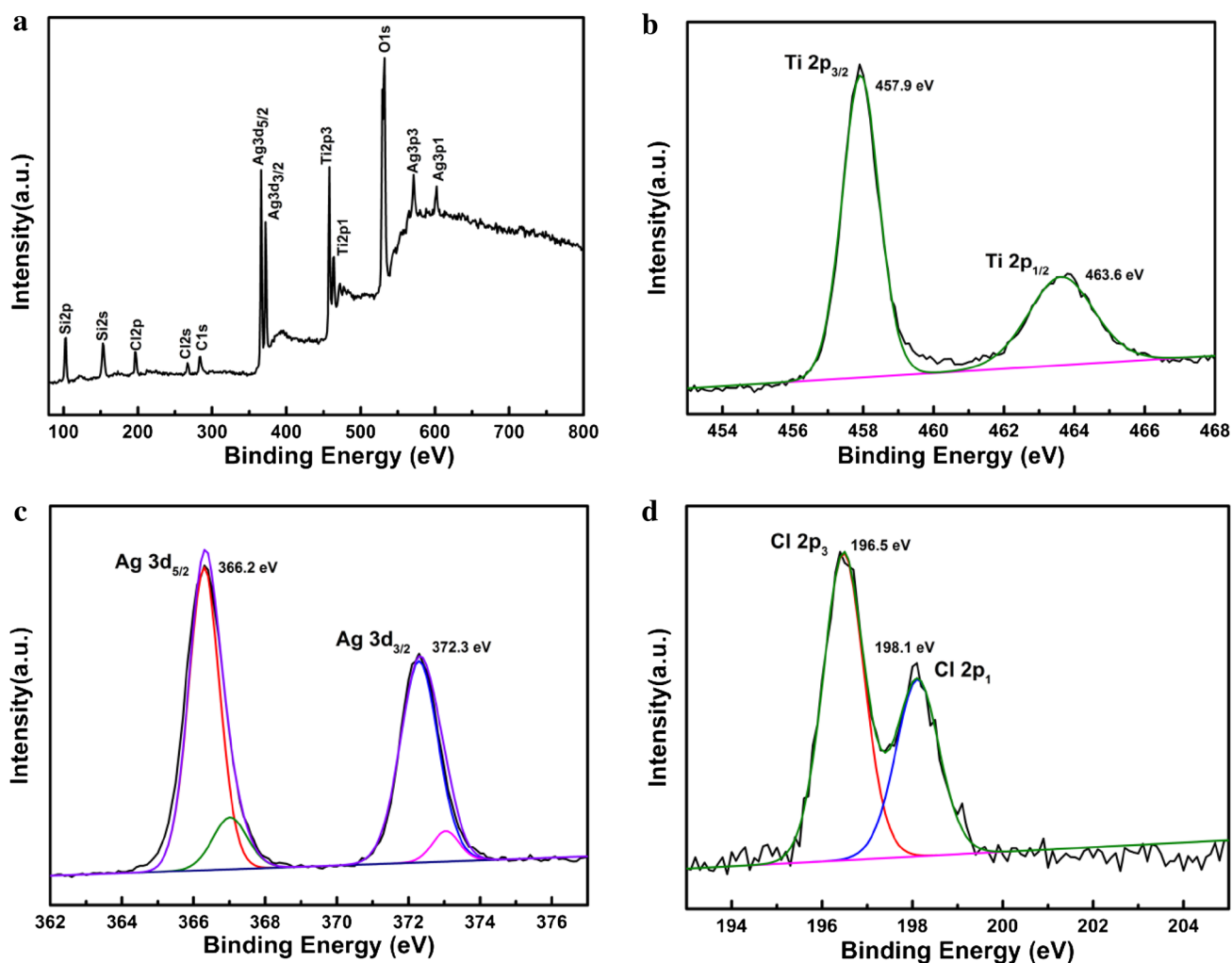


Fig. 6 XPS spectra of TiO_2 porous ceramic/Ag–AgCl-30 sample: **a** survey spectrum, **b** Ti 2p peaks, **c** Ag 3d peaks and **d** Cl 2p peaks

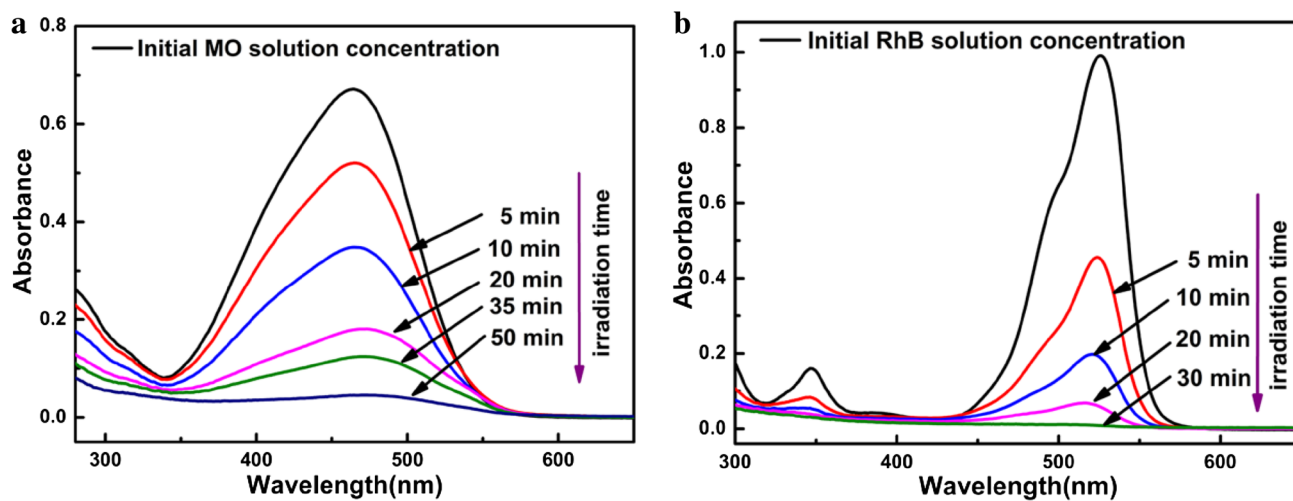


Fig. 7 UV–Vis adsorption spectra for the degradation of **a** MO and **b** RhB over TiO_2 porous ceramic/Ag–AgCl-30 under visible light irradiation

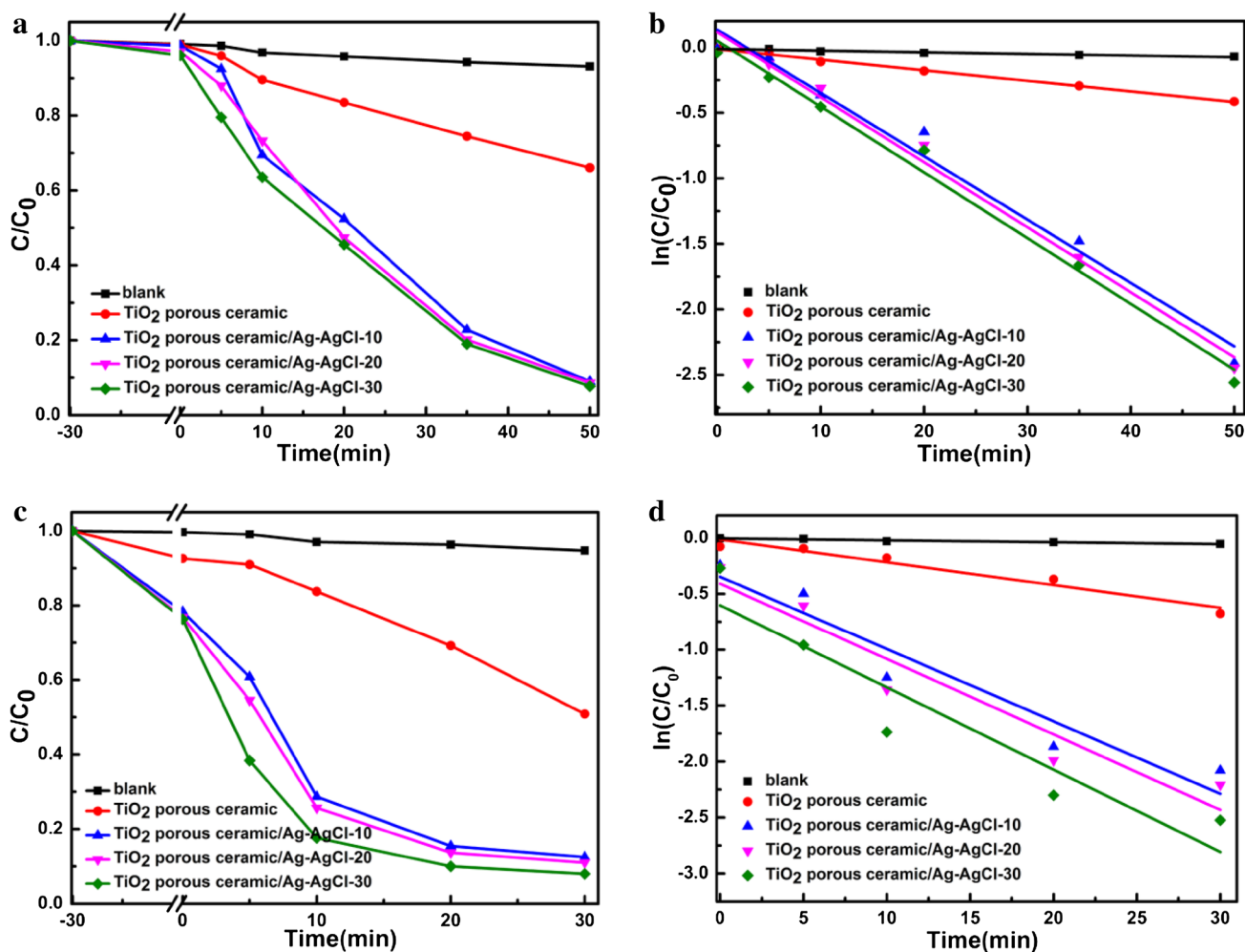


Fig. 8 Comparison of photocatalytic activity for the degradation of MO (a) and RhB (c) under visible light irradiation; Plot of $\ln(C/C_0)$ versus irradiation time of the different samples for the degradation of MO (b) and RhB (d) under visible light irradiation

Nearly 95% MO and 90% RhB molecules were degraded over TiO₂ porous ceramic/Ag–AgCl catalysts. This is contrasted with bare TiO₂ bulk which only achieved a 25% MO and 50% RhB degradations under identical conditions.

The photocatalytic degradation process of MO and RhB is described by first-order kinetics [33, 34] as expressed by: $\ln(C/C_0) = k_{app}t$, where k_{app} is the apparent rate constant, C_0 and C are the concentrations of MO or RhB solutions at time of 0 and t , respectively. The pseudo-first-rate kinetic rate constant can be deduced from the linear fitting of $\ln(C_0/C)$ versus irradiation time. As shown in Fig. 8b, d, there is a linear correlation between $\ln(C/C_0)$ and the irradiation time (t). TiO₂ porous ceramic/Ag–AgCl-30 showed the best photocatalytic activity ($k_{app} = 0.0502 \text{ min}^{-1}$ of MO, $k_{app} = 0.0735 \text{ min}^{-1}$ of RhB). The k_{app} values of different TiO₂ porous ceramic/Ag–AgCl catalysts were similar, and this was in accord with the photocatalytic activity.

The MO or RhB photocatalytic activities of TiO₂ porous ceramic/Ag–AgCl-30 composite are 6.25 times or 3.62 times higher than that of TiO₂ porous ceramic.

In addition to high photocatalytic activity, the stability of photocatalysts is a vital concern for practical application. The stability of TiO₂ porous ceramic/Ag–AgCl was evaluated by cycled degradation of MO and RhB with identical conditions for four times under visible light irradiation, each time the tested samples were washed with de-ionized water and dried at room temperature before the next test. The photocatalyst exhibited virtually no decline of activity after four cycles of degradations of MO and RhB, as shown in Fig. 9a, b. Fig. 9c shows that the cubic morphology of AgCl nanoparticles distributed on the TiO₂ porous ceramic surface remained intact after four cycles. The results demonstrated that the photocatalysts were effective and stable under cycled degradations of MO and RhB with visible light irradiation.

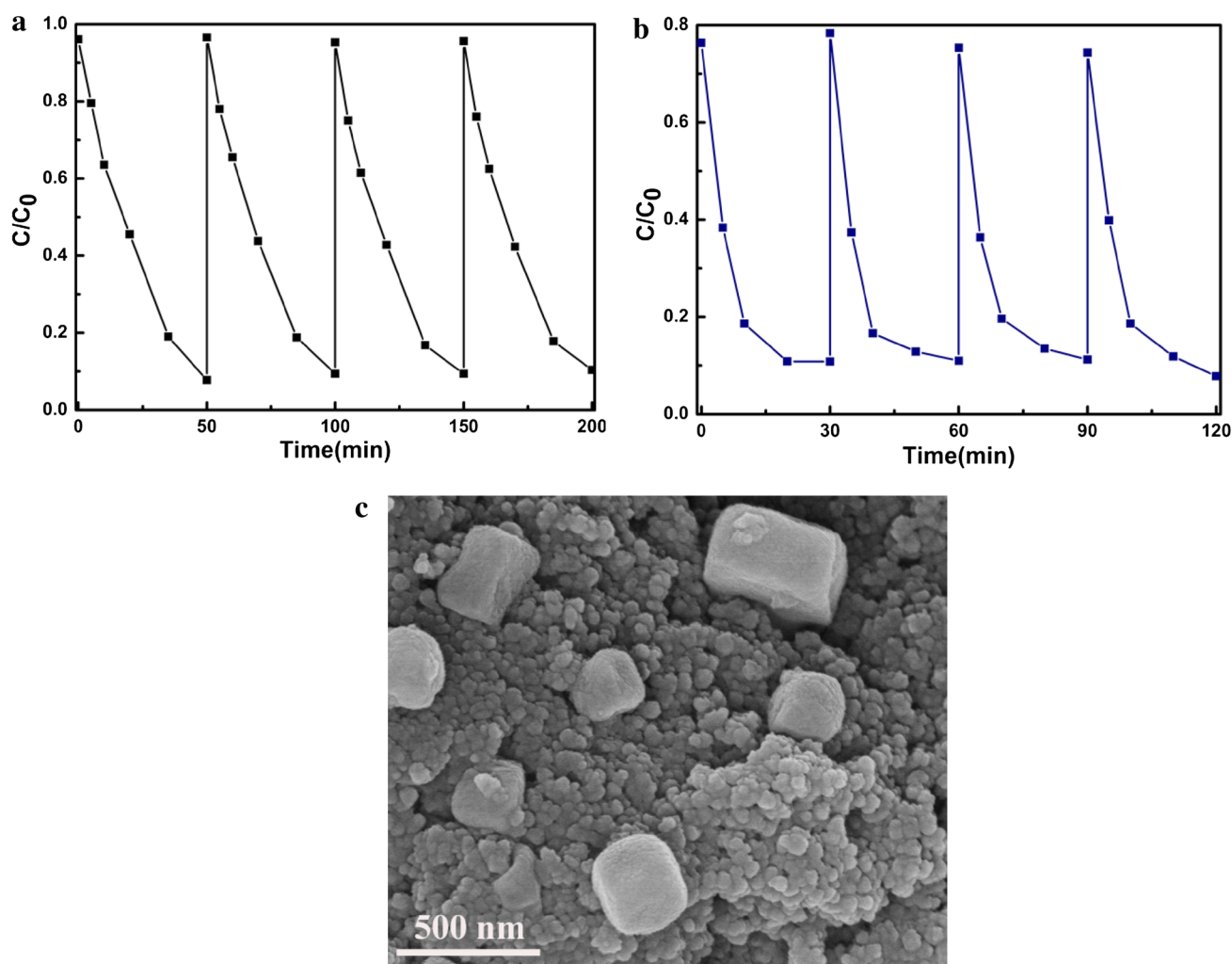


Fig. 9 Cycling degradation curves of **a** MO and **b** RhB aqueous solutions over TiO₂ porous ceramic/Ag–AgCl-30 under visible light irradiation; **c** SEM image of TiO₂ porous ceramic/Ag–AgCl-30 used after four cycling experiments

3.3 Formation of hydroxyl radicals

The fluorescence emission spectrum (excitation at 315 nm) of terephthalic acid solution was measured during visible light irradiation. Figure 10 shows the PL intensity of 2-hydroxyterephthalic acid. As shown in the Fig. 10, gradual increase in the fluorescence intensity at about 425 nm was observed with increasing irradiation time over TiO₂ porous ceramic/Ag–AgCl-30. When the system was in the absence of visible light, no PL intensity was observed. Hence, it was reasonable to conclude that the reaction between terephthalic acid and ·OH produces fluorescence.

4 Conclusion

We have demonstrated a novel method to prepare TiO₂ porous ceramic/Ag–AgCl by mixing P25 TiO₂ powder with

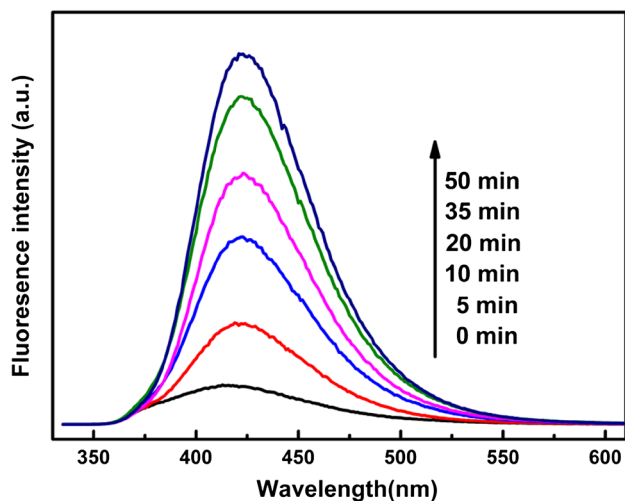


Fig. 10 Fluorescence spectral changes observed during illumination of TiO₂ porous ceramic/Ag–AgCl-30 in a 5×10^{-4} M terephthalic acid aqueous solution under visible light irradiation

silica gel, pressing, sintering and subsequent precipitation of AgCl and photochemical reduction. The TiO₂ bulk matrix was chemically stable and porous with abundant pores after sintering. The highly porous nature of the TiO₂ bulk facilitated implantation of AgCl NPs. TiO₂ porous ceramic/Ag–AgCl composite exhibited enhanced photocatalytic activity and stability in the degradation of MO and RhB under visible light irradiation. The reaction rate constants of MO or RhB degradation over the TiO₂ porous ceramic/Ag–AgCl (0.0502, 0.0735 min⁻¹) are much faster than bare TiO₂ porous ceramic (0.0081, 0.0203 min⁻¹) under visible light irradiation. As a result, the enhanced photocatalytic activity can be interpreted by the synergistic effect of TiO₂ and Ag–AgCl, as well as surface plasmon resonance of Ag⁰. The study offers a novel composite photocatalyst that has real potential for industrial applications, and it may also provide a simple methodology for preparing other visible light driven porous ceramic/Ag–AgCl photocatalysts.

Acknowledgements The authors are grateful to the scientific research foundation of Nanjing University of Science and Technology (AE89909) and the Priority Academic Program Development of Jiangsu Higher Education Institutions for financial support.

Open Access This article is distributed under the terms of the Creative Commons Attribution 4.0 International License (<http://creativecommons.org/licenses/by/4.0/>), which permits unrestricted use, distribution, and reproduction in any medium, provided you give appropriate credit to the original author(s) and the source, provide a link to the Creative Commons license, and indicate if changes were made.

References

1. D. Chen, T. Li, Q. Chen, Hierarchically plasmonic photocatalysts of Ag/AgCl nanocrystals coupled with single-crystalline WO₃ nanoplates. *Nanoscale* **4**, 5431–5439 (2012)
2. A. Fujishima, K. Honda, Electrochemical photolysis of water at a semiconductor electrode. *Nature* **238**, 37–38 (1972)
3. M.R. Hoffmann, S.T. Martin, W. Choi, Environmental applications of semiconductor photocatalysis. *Chem. Rev.* **95**, 69–96 (1995)
4. J. Yu, S. Liu, H. Yu, Microstructures and photoactivity of mesoporous anatase hollow microspheres fabricated by fluoride-mediated self-transformation. *J. Catal.* **249**, 59–66 (2007)
5. X.Z. Li, F.B. Li, Study of Au/Au³⁺-TiO₂ photocatalysts toward visible photooxidation for water and wastewater treatment. *Environ. Sci. Technol.* **35**, 2381–2387 (2001)
6. J.G. Yu, Y.R. Su, B. Cheng, Template-free fabrication and enhanced photocatalytic activity of hierarchical macro-/mesoporous titania. *Adv. Funct. Mater.* **17**, 1984–1990 (2007)
7. J. Choi, H. Park, M.R. Hoffmann, Combinatorial doping of TiO₂ with platinum (Pt), chromium (Cr), vanadium (V), and nickel (Ni) to achieve enhanced photocatalytic activity with visible light irradiation. *J. Mater. Res.* **25**, 149–158 (2010)
8. R. Asahi, T. Morikawa, T. Ohwaki, Visible-light photocatalysis in nitrogen-doped titanium oxides. *Science* **293**, 269–271 (2001)
9. L.G.C. Rego, R. Silva, J.A. Freire, Visible light sensitization of TiO₂ surfaces with Alq₃ complexes. *J. Phys. Chem. C* **114**, 1317–1325 (2009)
10. Y. Bi, S. Ouyang, N. Umezawa, J. Gao, J. Ye, Facet effect of single-crystalline Ag₃PO₄ sub-microcrystals on photocatalytic properties. *J. Am. Chem. Soc.* **133**, 6490–6492 (2011)
11. Y. Hou, B.L. Abrams, P.C.K. Vesborg, Bioinspired molecular co-catalysts bonded to a silicon photocathode for solar hydrogen evolution. *Nat. Mater.* **10**, 434–438 (2011)
12. J.J. Storhoff, R. Elghanian, R.C. Mucic, C.A. Mirkin, R.L. Letsinger, One-pot colorimetric differentiation of polynucleotides with single base imperfections using gold nanoparticle probes. *J. Am. Chem. Soc.* **120**, 1959–1964 (1998)
13. Y. Tian, T. Tatsuma, Plasmon-induced photoelectrochemistry at metal nanoparticles supported on nanoporous TiO₂. *Chem. Commun.* **16**, 1810–1811 (2004)
14. K. Awazu, M. Fujimaki, C. Rockstuhl, J. Tominaga, H. Murakami, Y. Ohki, N. Yoshida, T. Watanabe, A plasmonic photocatalyst consisting of silver nanoparticles embedded in titanium dioxide. *J. Am. Chem. Soc.* **130**, 1676–1680 (2008)
15. P. Wang, T.F. Xie, H.Y. Li, L. Peng, Y. Zhang, T.S. Wu, S. Pang, Y.F. Zhao, D.J. Wang, Synthesis and plasmon-induced charge-transfer properties of monodisperse gold-doped titania microspheres. *Chem. Eur. J.* **15**, 4366–4372 (2009)
16. G. Zhao, H. Kozuka, T. Yoko, Sol-gel preparation and photoelectrochemical properties of TiO₂ films containing Au and Ag metal particles. *Thin Solid Films* **277**, 147–154 (1996)
17. E. Bae, W. Choi, Highly enhanced photoreductive degradation of perchlorinated compounds on dye-sensitized metal/TiO₂ under visible light. *Environ. Sci. Technol.* **37**, 147–152 (2003)
18. J. Liao, K. Zhang, L. Wang, Facile hydrothermal synthesis of heart-like Ag@AgCl with enhanced visible light photocatalytic performance. *Mater. Lett.* **83**, 136–139 (2012)
19. P. Wang, B. Huang, Z. Lou, Synthesis of highly efficient Ag@AgCl plasmonic photocatalysts with various structures. *Chem. Eur. J.* **16**, 538–544 (2010)
20. M. Zhu, P. Chen, M. Liu, Highly efficient visible-light-driven plasmonic photocatalysts based on graphene oxide-hybridized one-dimensional Ag/AgCl heteroarchitectures. *J. Mater. Chem.* **22**, 21487–21494 (2012)
21. J. Jiang, L. Zhang, Rapid Microwave-assisted nonaqueous synthesis and growth mechanism of AgCl/Ag, and its daylight-driven plasmonic photocatalysis. *Chem. Eur. J.* **17**, 3710–3717 (2011)
22. L. Han, P. Wang, C. Zhu, Y. Zhai, S. Dong, Facile solvothermal synthesis of cube-like Ag@AgCl: a highly efficient visible light photocatalyst. *Nanoscale* **3**, 2931–2935 (2011)
23. P. Wang, B. Huang, X. Qin, X. Zhang, Y. Dai, Ag@AgCl: a highly efficient and stable photocatalyst active under visible light. *Angew. Chem. Int. Ed.* **47**, 7931–7933 (2008)
24. C. Hu, Y. Lan, J. Qu, X. Hu, A. Wang, Ag/AgBr/TiO₂ visible light photocatalyst for destruction of azodyes and bacteria. *J. Phys. Chem. B* **110**, 4066–4072 (2006)
25. J.G. Yu, G.P. Dai, B.B. Huang, Fabrication and characterization of visible-light-driven plasmonic photocatalyst Ag/AgCl/TiO₂ nanotube arrays. *J. Phys. Chem. C* **113**, 16394–16401 (2009)
26. W.T. Liu, D.L. Chen, S.H. Yoo, S.O. Cho, Hierarchical visible-light-response Ag/AgCl@TiO₂ plasmonic photocatalysts for organic dye degradation. *Nanotechnology* **24**, 405706 (2013)
27. D. Chen, F. Huang, Y.B. Cheng, Mesoporous anatase TiO₂ beads with high surface areas and controllable pore sizes: a superior candidate for high-performance dye-sensitized solar cells. *Adv. Mater.* **21**, 2206–2210 (2009)
28. J.S. Lee, K.H. You, C.B. Park, Highly photoactive, low bandgap TiO₂ nanoparticles wrapped by graphene. *Adv. Mater.* **24**, 1084–1088 (2012)

29. B. Erdem, R.A. Hunsicker, G.W. Simmons, XPS and FTIR surface characterization of TiO₂ particles used in polymer encapsulation. *Langmuir* **17**, 2664–2669 (2001)
30. M. Ramstedt, P. Franklyn, Difficulties in determining valence for Ag⁰ nanoparticles using XPS-characterization of nanoparticles inside poly (3-sulphopropyl methacrylate) brushes, *Surf. Interface. Anal.* **42**, 855–858 (2010)
31. M. Zhu, P. Chen, M. Liu, Graphene oxide enwrapped Ag/AgX (X=Br, Cl) nanocomposite as a highly efficient visible-light plasmonic photocatalyst. *ACS Nano* **5**, 4529–4536 (2011)
32. D. Chen, S.H. Yoo, Q. Huang, G. Ali, S.O. Cho, Sonochemical synthesis of Ag/AgCl nanotubes and their efficient visible-light-driven photocatalytic performance. *Chem. Eur. J.* **18**, 5192–5200 (2012)
33. R. Li, H. Han, F. Zhang, D. Wang, C. Li, Highly efficient photocatalysts constructed by rational assembly of dual-cocatalysts separately on different facets of BiVO₄. *Energy Environ. Sci.* **7**, 1369–1376 (2014)
34. S. Han, L. Hu, N. Gao, A.A. Al-Ghamdi, X. Fang, Efficient self-assembly synthesis of uniform CdS spherical nanoparticles-Au nanoparticles hybrids with enhanced photoactivity. *Adv. Funct. Mater* **24**, 3725–3733 (2014)